



IceCube Search for Neutrinos Coincident with Compact Binary Mergers from LIGO-Virgo's First Gravitational-wave Transient Catalog

M. G. Aartsen¹, M. Ackermann², J. Adams¹, J. A. Aguilar³, M. Ahlers⁴, M. Ahrens⁵, C. Alispach⁶, K. Andeen⁷, T. Anderson⁸, I. Ansseau³, G. Anton⁹, C. Argüelles¹⁰, J. Auffenberg¹¹, S. Axani¹⁰, H. Bagherpour¹, X. Bai¹², A. Balagopal V.¹³, A. Barbano⁶, I. Bartos^{14,62}, S. W. Barwick¹⁵, B. Bastian², V. Baum¹⁶, S. Baur³, R. Bay¹⁷, J. J. Beatty^{18,19}, K.-H. Becker²⁰, J. Becker Tjus²¹, S. BenZvi²², D. Berley²³, E. Bernardini^{2,59}, D. Z. Besson^{24,60}, G. Binder^{17,25}, D. Bindig²⁰, E. Blaufuss²³, S. Blot², C. Boehm⁵, S. Böser¹⁶, O. Botner²⁶, J. Böttcher¹¹, E. Bourbeau⁴, J. Bourbeau²⁷, F. Bradascio², J. Braun²⁷, S. Bron⁶, J. Brostean-Kaiser², A. Burgman²⁶, J. Buscher¹¹, R. S. Busse²⁸, T. Carver⁶, C. Chen²⁹, E. Cheung²³, D. Chirkin²⁷, S. Choi³⁵, B. A. Clark³¹, K. Clark³², L. Classen²⁸, A. Coleman³³, G. H. Collin¹⁰, J. M. Conrad¹⁰, P. Coppin³⁴, K. R. Corley³⁵, P. Correa³⁴, S. Countryman³⁵, D. F. Cowen^{8,36}, R. Cross²², P. Dave²⁹, C. De Clercq³⁴, J. J. DeLaunay⁸, H. Dembinski³³, K. Deoskar⁵, S. De Ridder³⁷, P. Desiati²⁷, K. D. de Vries³⁴, G. de Wasseige³⁴, M. de With³⁸, T. DeYoung³¹, A. Diaz¹⁰, J. C. Díaz-Vélez²⁷, H. Djumovic¹³, M. Dunkman⁸, E. Dvorak¹⁷, B. Eberhardt²⁷, T. Ehrhardt¹⁶, P. Eller¹³, R. Engel²³, P. A. Evenson³³, S. Fahey²⁷, A. R. Fazely³⁹, J. Felde²³, K. Filimonov¹⁷, C. Finley⁵, D. Fox³⁶, A. Franckowiak², E. Friedman²³, A. Fritz¹⁶, T. K. Gaisser³³, J. Gallagher⁴⁰, E. Ganster¹¹, S. Garrappa², L. Gerhardt²⁵, K. Ghorbani²⁷, T. Glauch¹¹, T. Glüsenkamp⁹, A. Goldschmidt²⁵, J. G. Gonzalez³³, D. Grant³¹, T. Grégoire⁸, Z. Griffith²⁷, S. Griswold²², M. Günder¹¹, M. Gündüz²¹, C. Haack¹¹, A. Hallgren²⁶, R. Halliday³¹, L. Halve¹¹, F. Halzen²⁷, K. Hanson²⁷, A. Haungs¹³, D. Hebecker³⁸, D. Heereman³, P. Heix¹¹, K. Helbing²⁰, R. Hellauer²³, F. Henningsen⁴¹, S. Hickford²⁰, J. Hignight⁴², G. C. Hill⁴³, K. D. Hoffman²³, R. Hoffmann²⁰, T. Hoinka⁴⁴, B. Hokanson-Fasig²⁷, K. Hoshina^{27,61}, F. Huang⁸, M. Huber⁴¹, T. Huber^{2,13}, K. Hultqvist⁵, M. Hünnefeld⁴⁴, R. Hussain²⁷, S. In³⁰, N. Iovine³, A. Ishihara⁴⁵, M. Jansson⁵, G. S. Japaridze⁴⁶, M. Jeong³⁰, K. Jero²⁷, B. J. P. Jones⁴⁷, F. Jonske¹¹, R. Joppe¹¹, D. Kang¹³, W. Kang³⁰, A. Kappes²⁸, D. Kappesser¹⁶, T. Karg², M. Karl⁴¹, A. Karle²⁷, U. Katz⁹, M. Kauer²⁷, A. Keivani³⁵, M. Kellermann¹¹, J. L. Kelley²⁷, A. Kheirandish⁸, J. Kim³⁰, T. Kintscher², J. Kiryluk⁴⁸, T. Kittler⁹, S. R. Klein^{17,25}, R. Koirala³³, H. Kolanoski³⁸, L. Köpke¹⁶, C. Kopper³¹, S. Kopper⁴⁹, D. J. Koskinen⁴, M. Kowalski^{2,38}, K. Krings⁴¹, G. Krückl¹⁶, N. Kulacz⁴², N. Kurahashi⁵⁰, A. Kyriacou⁴³, J. L. Lanfranchi⁸, M. J. Larson²³, F. Lauber²⁰, J. P. Lazar²⁷, K. Leonard²⁷, A. Leszczyńska¹³, Q. R. Liu²⁷, E. Lohfink¹⁶, C. J. Lozano Mariscal²⁸, L. Lu⁴⁵, F. Lucarelli⁶, A. Ludwig⁵¹, J. Lünemann³⁴, W. Luszczak²⁷, Y. Lyu^{17,25}, W. Y. Ma², J. Madsen⁵², G. Maggi³⁴, K. B. M. Mahn³¹, Y. Makino⁴⁵, P. Mallik¹¹, K. Mallot²⁷, S. Mancina²⁷, I. C. Mariş³, S. Marka³⁵, Z. Marka³⁵, R. Maruyama⁵³, K. Mase⁴⁵, R. Maunu²³, F. McNally⁵⁴, K. Meagher²⁷, M. Medici⁴, A. Medina¹⁹, M. Meier⁴⁴, S. Meighen-Berger⁴¹, G. Merino²⁷, T. Meures³, J. Micallef³¹, D. Mockler³, G. Momente¹⁶, T. Montaruli⁶, R. W. Moore⁴², R. Morse²⁷, M. Moulai¹⁰, P. Muth¹¹, R. Nagai⁴⁵, U. Naumann²⁰, G. Neer³¹, L. V. Nguyen³¹, H. Niederhausen⁴¹, M. U. Nisa³¹, S. C. Nowicki³¹, D. R. Nygren²⁵, A. Obertacke Pollmann²⁰, M. Oehler¹³, A. Olivas²³, A. O'Murchadha³, E. O'Sullivan⁵, T. Palczewski^{17,25}, H. Pandya³³, D. V. Pankova⁸, N. Park²⁷, P. Peiffer¹⁶, C. Pérez de los Heros²⁶, S. Philippen¹¹, D. Pieloth⁴⁴, S. Pieper²⁰, E. Pinat³, A. Pizzuto²⁷, M. Plum⁷, A. Porcelli³⁷, P. B. Price¹⁷, G. T. Przybylski²⁵, C. Raab³, A. Raissi¹, M. Rameez⁴, L. Rauch², K. Rawlins⁵⁵, I. C. Rea⁴¹, A. Rehman³³, R. Reimann¹¹, B. Relethford⁵⁰, M. Renschler¹³, G. Renzi³, E. Resconi⁴¹, W. Rhode⁴⁴, M. Richman⁵⁰, S. Robertson²⁵, M. Rongen¹¹, C. Rott³⁰, T. Ruhe⁴⁴, D. Ryckbosch³⁷, D. Rysewyk Cantu³¹, I. Safa²⁷, S. E. Sanchez Herrera³¹, A. Sandrock⁴⁴, J. Sandroos¹⁶, M. Santander⁴⁹, S. Sarkar⁵⁶, S. Sarkar⁴², K. Satalecka², M. Schaufel¹¹, H. Schieler¹³, P. Schlunder⁴⁴, T. Schmidt²³, A. Schneider²⁷, J. Schneider⁹, F. G. Schröder^{13,33}, L. Schumacher¹¹, S. Sclafani⁵⁰, D. Seckel³³, S. Seunarine⁵², S. Shefali¹¹, M. Silva²⁷, R. Snihur²⁷, J. Soedingrekso⁴⁴, D. Soldin³³, M. Song²³, G. M. Spiczak⁵², C. Spiering², J. Stachurska², M. Stamatikos¹⁹, T. Stanev³³, R. Stein², J. Stettner¹¹, A. Steuer¹⁶, T. Stezelberger²⁵, R. G. Stokstad²⁵, A. Stöbl⁴⁵, N. L. Strotjohann², T. Stürwald¹¹, T. Stuttard⁴, G. W. Sullivan²³, I. Taboada²⁹, F. Tenholt²¹, S. Ter-Antonyan³⁹, A. Terliuk², S. Tilav³³, K. Tollefson³¹, L. Tomankova²¹, C. Tönnis⁵⁷, S. Toscano³, D. Tosi²⁷, A. Trettin², M. Tselengidou⁹, C. F. Tung²⁹, A. Turcati⁴¹, R. Turcotte¹³, C. F. Turley⁸, B. Ty²⁷, E. Unger²⁶, M. A. Unland Elorrieta²⁸, M. Usner², J. Vandenbroucke²⁷, W. Van Driessche³⁷, D. van Eijk²⁷, N. van Eijndhoven³⁴, J. van Santen², S. Verpoest³⁷, D. Veske³⁵, M. Vraeghe³⁷, C. Walck⁵, A. Wallace⁴³, M. Wallraff¹¹, N. Wandkowsky²⁷, T. B. Watson⁴⁷, C. Weaver⁴², A. Weindl¹³, M. J. Weiss⁸, J. Weldert¹⁶, C. Wendt²⁷, J. Werthebach²⁷, B. J. Whelan⁴³, N. Whitehorn⁵¹, K. Wiebe¹⁶, C. H. Wiebusch¹¹, L. Wille²⁷, D. R. Williams⁴⁹, L. Wills⁵⁰, M. Wolf⁴¹, J. Wood²⁷, T. R. Wood⁴², K. Woschnagg¹⁷, G. Wrede⁹, D. L. Xu²⁷, X. W. Xu³⁹, Y. Xu⁴⁸, J. P. Yanez⁴², G. Yodh^{15,58}, S. Yoshida⁴⁵, T. Yuan²⁷, and M. Zöcklein¹¹

¹ Department of Physics and Astronomy, University of Canterbury, Private Bag 4800, Christchurch, New Zealand

² DESY, D-15738 Zeuthen, Germany

³ Université Libre de Bruxelles, Science Faculty CP230, B-1050 Brussels, Belgium

⁴ Niels Bohr Institute, University of Copenhagen, DK-2100 Copenhagen, Denmark

⁵ Oskar Klein Centre and Department of Physics, Stockholm University, SE-10691 Stockholm, Sweden

⁶ Département de physique nucléaire et corpusculaire, Université de Genève, CH-1211 Genève, Switzerland

⁷ Department of Physics, Marquette University, Milwaukee, WI 53201, USA

⁸ Department of Physics, Pennsylvania State University, University Park, PA 16802, USA

⁹ Erlangen Centre for Astroparticle Physics, Friedrich-Alexander-Universität Erlangen-Nürnberg, D-91058 Erlangen, Germany

¹⁰ Department of Physics, Massachusetts Institute of Technology, Cambridge, MA 02139, USA

¹¹ III. Physikalisches Institut, RWTH Aachen University, D-52056 Aachen, Germany

¹² Physics Department, South Dakota School of Mines and Technology, Rapid City, SD 57701, USA

- ¹³ Karlsruhe Institute of Technology, Institut für Kernphysik, D-76021 Karlsruhe, Germany
¹⁴ Department of Physics, University of Florida, Gainesville, FL 32611-8440, USA
¹⁵ Department of Physics and Astronomy, University of California, Irvine, CA 92697, USA
¹⁶ Institute of Physics, University of Mainz, Staudinger Weg 7, D-55099 Mainz, Germany
¹⁷ Department of Physics, University of California, Berkeley, CA 94720, USA
¹⁸ Department of Astronomy, Ohio State University, Columbus, OH 43210, USA
¹⁹ Department of Physics, and Center for Cosmology and Astro-Particle Physics, Ohio State University, Columbus, OH 43210, USA
²⁰ Department of Physics, University of Wuppertal, D-42119 Wuppertal, Germany
²¹ Fakultät für Physik & Astronomie, Ruhr-Universität Bochum, D-44780 Bochum, Germany
²² Department of Physics and Astronomy, University of Rochester, Rochester, NY 14627, USA
²³ Department of Physics, University of Maryland, College Park, MD 20742, USA
²⁴ Department of Physics and Astronomy, University of Kansas, Lawrence, KS 66045, USA
²⁵ Lawrence Berkeley National Laboratory, Berkeley, CA 94720, USA
²⁶ Department of Physics and Astronomy, Uppsala University, Box 516, S-75120 Uppsala, Sweden
²⁷ Department of Physics and Wisconsin IceCube Particle Astrophysics Center, University of Wisconsin, Madison, WI 53706, USA
²⁸ Institut für Kernphysik, Westfälische Wilhelms-Universität Münster, D-48149 Münster, Germany
²⁹ School of Physics and Center for Relativistic Astrophysics, Georgia Institute of Technology, Atlanta, GA 30332, USA
³⁰ Department of Physics, Sungkyunkwan University, Suwon 16419, Korea
³¹ Department of Physics and Astronomy, Michigan State University, East Lansing, MI 48824, USA
³² SNOLAB, 1039 Regional Road 24, Creighton Mine 9, Lively, ON, P3Y 1N2, Canada
³³ Bartol Research Institute and Department of Physics and Astronomy, University of Delaware, Newark, DE 19716, USA
³⁴ Vrije Universiteit Brussel (VUB), Dienst ELEM, B-1050 Brussels, Belgium
³⁵ Department of Physics, Columbia University, New York, NY 10027, USA
³⁶ Department of Astronomy and Astrophysics, Pennsylvania State University, University Park, PA 16802, USA
³⁷ Department of Physics and Astronomy, University of Gent, B-9000 Gent, Belgium
³⁸ Institut für Physik, Humboldt-Universität zu Berlin, D-12489 Berlin, Germany
³⁹ Department of Physics, Southern University, Baton Rouge, LA 70813, USA
⁴⁰ Department of Astronomy, University of Wisconsin, Madison, WI 53706, USA
⁴¹ Physik-department, Technische Universität München, D-85748 Garching, Germany
⁴² Department of Physics, University of Alberta, Edmonton, AB, T6G 2E1, Canada
⁴³ Department of Physics, University of Adelaide, Adelaide, 5005, Australia
⁴⁴ Department of Physics, TU Dortmund University, D-44221 Dortmund, Germany
⁴⁵ Department of Physics and Institute for Global Prominent Research, Chiba University, Chiba 263-8522, Japan
⁴⁶ CTSPS, Clark-Atlanta University, Atlanta, GA 30314, USA
⁴⁷ Department of Physics, University of Texas at Arlington, 502 Yates Street, Science Hall Room 108, Box 19059, Arlington, TX 76019, USA
⁴⁸ Department of Physics and Astronomy, Stony Brook University, Stony Brook, NY 11794-3800, USA
⁴⁹ Department of Physics and Astronomy, University of Alabama, Tuscaloosa, AL 35487, USA
⁵⁰ Department of Physics, Drexel University, 3141 Chestnut Street, Philadelphia, PA 19104, USA
⁵¹ Department of Physics and Astronomy, UCLA, Los Angeles, CA 90095, USA
⁵² Department of Physics, University of Wisconsin, River Falls, WI 54022, USA
⁵³ Department of Physics, Yale University, New Haven, CT 06520, USA
⁵⁴ Department of Physics, Mercer University, Macon, GA 31207-0001, USA
⁵⁵ Department of Physics and Astronomy, University of Alaska Anchorage, 3211 Providence Drive, Anchorage, AK 99508, USA
⁵⁶ Department of Physics, University of Oxford, Parks Road, Oxford OX1 3PU, UK
⁵⁷ Institute of Basic Science, Sungkyunkwan University, Suwon 16419, Korea

Received 2020 April 17; revised 2020 June 15; accepted 2020 June 16; published 2020 July 17

Abstract

Using the IceCube Neutrino Observatory, we search for high-energy neutrino emission coincident with compact binary mergers observed by the LIGO and Virgo gravitational-wave (GW) detectors during their first and second observing runs. We present results from two searches targeting emission coincident with the sky localization of each GW event within a 1000 s time window centered around the reported merger time. One search uses a model-independent unbinned maximum-likelihood analysis, which uses neutrino data from IceCube to search for pointlike neutrino sources consistent with the sky localization of GW events. The other uses the Low-Latency Algorithm for Multi-messenger Astrophysics, which incorporates astrophysical priors through a Bayesian framework and includes LIGO-Virgo detector characteristics to determine the association between the GW source and the neutrinos. No significant neutrino coincidence is seen by either search during the first two observing runs of the LIGO-Virgo detectors. We set upper limits on the time-integrated neutrino emission within the 1000 s window for each of the 11 GW events. These limits range from 0.02 to 0.7 GeV cm⁻². We also set limits on the total isotropic equivalent energy, E_{iso} , emitted in high-energy neutrinos by each GW event. These limits range from 1.7×10^{51} to 1.8×10^{55} erg. We conclude with an outlook for LIGO-Virgo observing run O3, during which both analyses are running in real time.

Unified Astronomy Thesaurus concepts: [Neutrino astronomy \(1100\)](#); [High energy astrophysics \(739\)](#); [Gravitational waves \(678\)](#)

⁵⁸ Author is deceased.

⁵⁹ Also at Università di Padova, I-35131 Padova, Italy.

⁶⁰ Also at National Research Nuclear University, Moscow Engineering Physics Institute (MEPhI), Moscow 115409, Russia.

⁶¹ Earthquake Research Institute, University of Tokyo, Bunkyo, Tokyo 113-0032, Japan.

⁶² Alfred P. Sloan Research Fellow.

1. Introduction

The discovery of gravitational waves (GWs; Abbott et al. 2016) and astrophysical high-energy neutrinos has opened new opportunities for astrophysics with the possibility of finding multimessenger fingerprints (LIGO Collaboration & Virgo Collaboration 2008; Abbott et al. 2017a; Aartsen et al. 2018).

Both GW and high-energy neutrino detections are now reported on a weekly to monthly basis (AMON 2019; GraceDB 2019). All GW detections by the LIGO and Virgo observatories published to date are well understood in the context of coalescing compact binary systems (Aasi et al. 2015; Virgo Collaboration 2015; Abbott et al. 2019), while the dominant origin of the detected astrophysical neutrinos is less certain (Aartsen et al. 2020). The joint observation of GWs and high-energy neutrinos could shed light on the underlying source population responsible for neutrino emission and would give insight into the connection between the interaction of compact objects and the properties of energetic outflows driven by their interactions (Ando et al. 2013; Bartos et al. 2013). It could also shed light on astrophysical sources that are electromagnetically obscured due to a surrounding dense environment but transparent to neutrinos (Razzaque et al. 2003; Bartos et al. 2012; Kimura et al. 2018).

For over a decade, there has been a sustained effort dedicated to discovering joint sources of GWs and high-energy neutrinos (Aso et al. 2008; van Elewyck et al. 2009; Bartos et al. 2011; Baret et al. 2012; Adrián-Martínez et al. 2013; Ando et al. 2013; Aartsen et al. 2014; Adrián-Martínez et al. 2016; Albert et al. 2017a, 2017b). The first observational constraints on common sources were obtained from nondetections (Bartos et al. 2011). Initial LIGO-Virgo data were analyzed in two independent searches, one using ANTARES data (Adrián-Martínez et al. 2013) and the other using IceCube data (Aartsen et al. 2014). After the onset of the era of advanced GW detectors, GW discoveries led to an increased interest in finding neutrino counterparts of GWs (Adrián-Martínez et al. 2016; Albert et al. 2017a, 2017b; Abe et al. 2018; Avrorin et al. 2018; Petkov et al. 2018). Additionally, a subthreshold search looked for events where neither the GW nor the neutrino trigger could be independently confirmed to be astrophysical (Albert et al. 2019). No statistically significant correlations were found in these searches.

The near real-time availability of GW and high-energy neutrino data enables low-latency joint searches. This allows for follow-up observations within a few minutes of an alert, which is crucial for observing prompt emission with multiple messengers. The current Low-Latency Algorithm for Multimessenger Astrophysics (LLAMA) evolved from the previous joint GW–neutrino search pipeline (Baret et al. 2012) that produced the bulk of the published results to date. During the second LIGO-Virgo observing run (O2), LLAMA combined data from LIGO, Virgo, and IceCube and disseminated results to electromagnetic follow-up partners (Countryman et al. 2019). The application of LLAMA to the data from the O2 observing run provided the proof of concept for a reliable low-latency multimessenger pipeline. With an improved significance measure (Bartos et al. 2019), LLAMA continues to run during the current third observing run (Countryman et al. 2019; Keivani et al. 2019), together with the online version of the analysis using the maximum-likelihood method (Hussain et al. 2019) discussed below.

1.1. First and Second Observing Runs of the Advanced GW Detector Network

During the first and second observing runs of the advanced GW detector network (Aasi et al. 2015; Virgo Collaboration 2015), the LIGO and Virgo Collaborations (LVC) searched the collected data and discovered signals from compact binary mergers. Three binary black hole (BBH) mergers were detected during O1 (2015 September 12–2016 January 19), and an additional seven BBH events were detected during O2 (2016 November 30–2017 August 25). The LVC also discovered the very first binary neutron star (BNS) inspiral signal during O2, on 2017 August 17 (GW170817). A GW transient catalog of compact binary mergers observed by LIGO and Virgo during the first and second observing runs, GWTC-1, provides information on source properties and localization on the aforementioned 11 GW events (Abbott et al. 2019).

The observed masses of BBH components span a wide range from $7.7^{+2.2}_{-2.5}$ to $50.2^{+16.2}_{-10.2} M_{\odot}$, while for the BNS event, GW170817, the NS masses are $1.27^{+0.09}_{-0.09}$ and $1.46^{+0.12}_{-0.10} M_{\odot}$. The O1 and O2 GW events range in distance between 40^{+8}_{-15} Mpc for GW170817 and 2840^{+1400}_{-1360} Mpc for GW170729 (Abbott et al. 2019). All references to distance refer to the luminosity distance, D_L .

The time difference between the signals observed at the different interferometers in the GW detector network, together with the phase and amplitude of the detected GW events, enables sky localization of the source (Singer & Price 2016; Veitch et al. 2015). The 90% credible regions of the sky localizations for the GWTC-1 events span $16\text{--}1666 \text{ deg}^2$. Most events were observed only with the two LIGO detectors; thus, the corresponding sky localization regions for these events are rather large. The presence of the Virgo detector, especially for closer and/or higher-mass events, significantly improves the localization (see Table 1), though in all cases, the GW localization is poor with respect to the angular uncertainty of high-energy neutrino events, which tend to be less than a few square degrees.

IceCube and LIGO-Virgo have previously reported on the search for high-energy neutrino counterparts for four of the 11 GWTC-1 catalog events (GW150914, GW151012, and GW151226 from O1 and GW170817 from O2; Adrián-Martínez et al. 2016; Albert et al. 2017a, 2017b). Moreover, during O2, the LLAMA disseminated joint search results (Countryman et al. 2019) to electromagnetic follow-up partners for six events (GW170104, GW170608, GW170809, GW170814, GW170817, and GW170823), as well as for additional candidate events that were distributed to LVC partners (Abbott et al. 2019). In this paper, we present the results for all 11 GW events in the GWTC-1 catalog from a model-independent unbinned maximum-likelihood search, as well as an updated version of the previous LLAMA search.

Both searches presented below search for prompt neutrino emission within a 1000 s time window centered around the GW event time. This search window is chosen based on a range of neutrino emission mechanisms from gamma-ray bursts and is a conservative estimate of the difference in arrival times of the GW and neutrinos (Baret et al. 2011). Searches for longer-timescale neutrino emission are in development but are not considered here.

Table 1
Results for Every Detected GW from the O1 and O2 Observing Runs

O1 and O2 Detections										
Event	Type	Detectors	Ω (deg ²)	D_L (Mpc)	UL Range (GeV cm ⁻²)	p -value	Maximum Likelihood		LLAMA	
							UL (GeV cm ⁻²)	E_{iso} UL (erg)	p -value	UL (GeV cm ⁻²)
GW150914	BBH	LH	182	440^{+150}_{-170}	0.0296–1.03	0.51	0.66	5.10×10^{53}	0.29	0.70
GW151012	BBH	LH	1523	1080^{+550}_{-490}	0.0286–0.821	0.83	0.16	7.50×10^{53}	0.82	0.18
GW151226	BBH	LH	1033	450^{+180}_{-190}	0.0286–0.904	0.74	0.22	1.74×10^{53}	0.26	0.21
GW170104	BBH	LH	921	990^{+440}_{-430}	0.0286–0.667	0.54	0.044	1.81×10^{53}	0.16	0.055
GW170608	BBH	LH	392	320^{+120}_{-110}	0.0309–0.0821	0.61	0.037	1.37×10^{52}	0.97	0.038
GW170729	BBH	LHV	1041	2840^{+1400}_{-1360}	0.0286–1.02	0.21	0.62	1.80×10^{55}	0.17	0.62
GW170809	BBH	LHV	308	1030^{+320}_{-390}	0.0568–0.758	0.60	0.27	1.02×10^{54}	0.83	0.26
GW170814	BBH	LHV	87	600^{+150}_{-220}	0.488–0.711	0.83	0.45	5.47×10^{53}	1.0	0.43
GW170817	BNS	LHV	16	40^{+7}_{-15}	0.180–0.429	0.19	0.27	1.67×10^{51}	0.94	0.25
GW170818	BBH	LHV	39	1060^{+420}_{-380}	0.0364–0.0431	0.58	0.028	1.17×10^{53}	0.40	0.028
GW170823	BBH	LH	1666	1940^{+970}_{-900}	0.0286–0.796	0.75	0.18	2.33×10^{54}	0.25	0.18

Note. Here Ω is the area of the 90% credible region of the GW and D_L is the reported median luminosity distance. These values are taken from GWTC-1 (Abbott et al. 2019). The Detectors column indicates which of the three LIGO-Virgo detectors detected the GW. We also report 90% ULs on the energy-scaled time-integrated flux, E^2F , from both analyses. The UL Range column shows the minimum and maximum 90% ULs assuming a point-source hypothesis within the 90% credible region of the GW skymap. Here E_{iso} is the UL on the isotropic equivalent energy emitted in neutrinos during 1000 s. Note that error bars on derived energy quantities are not shown for clarity but are dominated by the error in the distance measurements of each GW.

1.2. IceCube

IceCube is a cubic-kilometer neutrino observatory located at the geographic South Pole (Aartsen et al. 2017a). IceCube consists of 86 strings, each of which holds 60 digital optical modules (DOMs) that are located at depths between 1.5 and 2.5 km in the Antarctic ice. These DOMs contain photo-multiplier tubes that detect the Cerenkov light radiated by charged secondaries of neutrino charged-current and neutral-current interactions.

IceCube’s sensitivity to a point source is strongly dependent on the decl. of the source. Figure 1 shows IceCube’s sensitivity to a transient point source in a 1000 s time window as a function of decl. The predominant background in the northern sky consists of atmospheric neutrinos that can travel large column depths through the Earth, while any atmospheric muons will be absorbed in the Earth (Formaggio & Zeller 2012). This is not the case in the southern sky, where atmospheric muons have enough energy to travel from the atmosphere to the detector, resulting in a much higher total background rate. Therefore, IceCube is much more sensitive to sources in the northern sky.

IceCube’s nearly 100% uptime and continuous 4π sr field of view make it an ideal observatory for multimessenger programs, both to trigger other observatories and to perform follow-ups (Aartsen et al. 2017b). In the case of multimessenger follow-ups of GW events, IceCube is able to search for neutrinos within the full GW localization region for all reported GW events.

Both analyses described in this paper use the same neutrino data, which come from the IceCube Gamma-ray Follow

Up (GFU) sample (Kintscher 2016), but they use different statistical methods and test different hypotheses. This sample is used for low-latency as well as offline analyses in IceCube. It consists of throughgoing muon tracks primarily induced by cosmic-ray interactions in the atmosphere. These backgrounds consist of downgoing muons as well as upgoing muons from atmospheric muon–neutrino interactions. The rate of background events in the sample is roughly 3 orders of magnitude larger than the rate of astrophysical neutrinos. Overall, the sample has a 6.7 mHz all-sky event rate, and the events in the sample have a median angular resolution of $\lesssim 1^\circ$ for energies above 1 TeV. The GFU sample is ideal for real-time multimessenger follow-ups due to its low latency (~ 30 s) and good angular resolution.

2. Methods

2.1. Unbinned Maximum Likelihood

The unbinned maximum-likelihood analysis tests for a pointlike neutrino source that is consistent with the localization of the GW source detected by LVC. The method uses the GW skymap as a spatial weight in a neutrino point-source likelihood (Schumacher 2019). The likelihood has the form

$$\mathcal{L} = \frac{e^{-(n_s+n_b)} (n_s+n_b)^N}{N!} \prod_{i=1}^N \frac{n_s \mathcal{S}_i + n_b \mathcal{B}_i}{n_s + n_b}, \quad (1)$$

where n_s is the number of signal events, n_b is the number of background events, and N is the total number of events in the sky. Here \mathcal{S}_i and \mathcal{B}_i are the signal and background probability distribution functions, respectively.

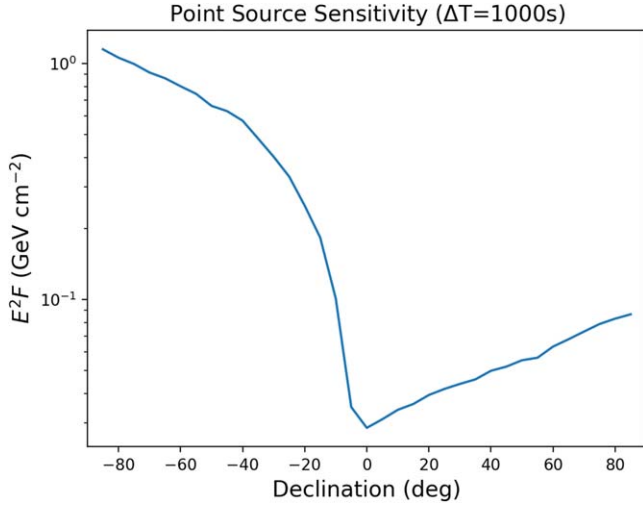


Figure 1. IceCube’s 90% C.L. sensitivity to a transient point source within 1000 s assuming an E^{-2} spectrum. We assume uniform emission within the time window. Here E^2F is the energy-scaled time-integrated flux, where the time-integrated flux is defined as $F = dN/dE dA$. The choice of an E^{-2} flux provides an optimistic limit on the sensitivity of IceCube and is motivated by Fermi acceleration.

The sky is divided into equal-area bins using HEALPix (Górski et al. 2005). The pixels are roughly 0.01 deg^2 , which is about the order of magnitude of the best angular resolution of the neutrino events in the GFU sample. In each pixel, the likelihood is maximized with respect to n_s and the source spectral index, γ .

The maximized likelihood, which represents the hypothesis most compatible with our data, is then multiplied by the spatial weight, which is a penalty at every pixel derived from the probability distribution of the GW event over the sky. This yields a weighted test statistic (TS)

$$\Lambda = 2 \ln \left(\frac{L(\hat{n}_s, \hat{\gamma}) \cdot w}{L(n_s = 0)} \right), \quad (2)$$

where w is the weight derived from the GW localization, $w = P_{\text{GW}}(\Omega)/A_{\text{pix}}$, where $P_{\text{GW}}(\Omega)$ is the GW localization probability as a function of position on the sky and A_{pix} is the area of the pixels on the sky. A full, detailed description of this method can be found in Hussain et al. (2019).

For a given GW event, we test for coincident neutrinos by considering a ± 500 s time window centered on the GW event time. To keep the analysis model-independent, neutrinos are assumed to be emitted uniformly within the ± 500 s time window. An example of a GW event overlaid with IceCube neutrinos within ± 500 s of the GW event is shown in Figure 2. For a gallery of all 11 skymaps with overlaid neutrinos, see Figure A4 in the Appendix.

We quantify the significance of a given observation by comparing our maximum observed Λ over the full sky to a background-only distribution and computing the resulting p -value. The background distribution is built from 30,000 trials using randomized neutrino events from the data themselves. To randomize the neutrino events used in each trial, the event arrival times are randomly shuffled while keeping the local coordinates of the events. This procedure preserves the time structure of the data set while assigning a random R.A. to each neutrino event, thus producing a unique

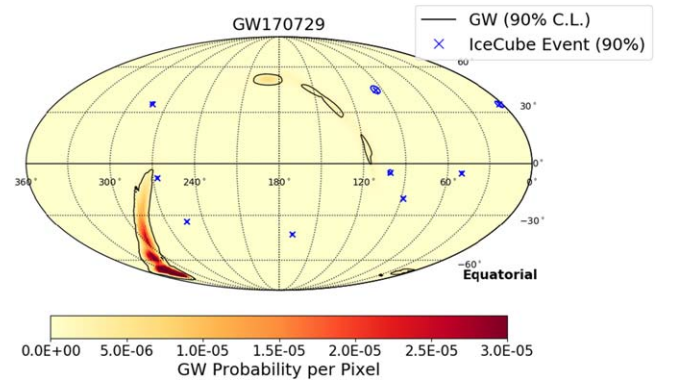


Figure 2. Example of a neutrino follow-up to GW170729 (Abbott et al. 2019), a BBH merger during the O2 observing run. Here the neutrinos observed within ± 500 s of the GW event are represented by blue crosses with 90% containment angular errors, and the GW localization PDF is shown in red, with the 90% credible region in black. Note that some of the 90% containment regions for the neutrinos are smaller than the blue crosses, so the error regions are not visible.

sample for each trial. For more details on this scrambling method, see Alexandreas et al. (1993) and Cassidy et al. (1989). An example of a background-only TS distribution for GW170729 is shown in Figure A1 in the Appendix. We fix the GW skymap for these trials so each GW event in the catalog has a unique background distribution. The associated p -value for a given GW event quantifies the chance probability of a set of background neutrinos having a significant correlation with the localization of the GW event. Thirty thousand trials per GW event yield enough statistics to compute accurate p -values while still being computationally feasible.

2.2. LLAMA

The LLAMA search calculates the odds ratio of having a multimessenger counterpart for a GW event versus the GW originating from noise or not having a counterpart (see Countryman et al. 2019; Keivani et al. 2019 for more information). This odds ratio is used as the TS for the search. The calculation of the odds ratio is based on a Bayesian framework by assuming a model for the multimessenger sources (Bartos et al. 2019). The method uses a distribution for the astrophysical high-energy neutrinos’ total emission energies, a spectrum for individual neutrinos’ differential energy density, IceCube’s detector response, and the spatial position reconstruction of the GW detection to estimate the expected number of neutrinos to be detected from the GW event. More neutrinos are expected to be detected from closer and otherwise identical events; thus, closer events are favored. A log-uniform distribution between 10^{46} and 10^{51} erg is used for the distribution of the total high-energy neutrino emission energy. The assumed neutrino emission spectrum is a power law with exponent $\gamma = -2$. The method’s input parameters are the detection times and localizations of candidate neutrinos and the GW, the reconstructed energies of the candidate neutrinos, the reconstructed distance of the GW, and the signal-to-noise ratio (S/N) of the GW. For GW events that have confirmed detections, as is the case with the 11 events considered here, the probability of the GW event arising from background is assumed to be zero, and the S/N information from the GW is not used. The method assumes neutrinos and GWs are emitted uniformly in ± 250 s around the joint astrophysical event time (Baret et al. 2011).

This results in a triangular distribution for the time difference between neutrinos and GWs with a maximum of ± 500 s time difference, where neutrinos temporally closer to the GW are favored. The p -value for each event is found by comparing the observed TS value for the event to a background distribution. The background distribution is built by running the analysis on injected GWs that are distributed uniformly in the comoving volume and detected with the sensitivity of the GW detectors during the O1 and O2 runs, which have similar sensitivities. The background distributions for BBH and BNS events are kept separate due to the significantly different distance distributions of their detections. Figure A3 in the Appendix shows the background TS distribution for BBH mergers detected with three GW detectors: aLIGO Hanford, aLIGO Livingston, and AdVirgo.

3. Results

No significant neutrino correlation was found for the 11 GWs in the O1 and O2 observing runs. We set upper limits (ULs) on the energy-scaled time-integrated flux, $E^2 F$, assuming an E^{-2} source spectrum. A single UL on $E^2 F$ is derived for each GW event. This is done via signal injection trials, which are described in detail in the Appendix. We also report a range of ULs for each GW event. This range corresponds to the minimum and maximum UL that IceCube can set within the 90% credible region of the GW event. The results are shown in Table 1.

We also compute a UL on an astrophysical quantity of interest, the isotropic equivalent energy, E_{iso} , assuming an E^{-2} source spectrum. Physically, this quantity represents the total energy emitted in neutrinos during the 1000 s time window, assuming spherically symmetric emission. E_{iso} encodes the intrinsic energy emitted by the source combined with the relative Doppler boost of the emission. Due to the uncertainties in the 3D localization of the GW source, we also marginalize over the 3D position of the source to get a marginalized UL on E_{iso} . This results in a single UL that encapsulates the significant uncertainties in the position of the source.

We relate E_{iso} to the neutrino flux observed by IceCube,

$$\begin{aligned} \frac{E_{\text{iso}}}{4\pi r^2} &= \int_{E_1}^{E_2} \Phi(E) E \Delta t dE \\ &= \Phi_0 \Delta t E_0^2 \ln \left(\frac{E_2}{E_1} \right), \end{aligned} \quad (3)$$

where we assume that the flux, $\Phi(E)$, follows a simple power-law spectrum, $\Phi(E) = \Phi_0 (E/E_0)^{-2}$. The flux normalization Φ_0 has units of $\text{GeV}^{-1} \text{cm}^{-2} \text{s}^{-1}$. The power-law flux is related to the flux defined in Figure 1 as $E^2 F = E^2 \Phi(E) \Delta t$. Here E_1 and E_2 are the minimum and maximum energy of the neutrino Monte Carlo sample, respectively, where $E_1 = 10$ and $E_2 = 10^{9.5}$ GeV. Thus, our E_{iso} ULs are to be taken as limits on the energy emitted in neutrinos between E_1 and E_2 .

Next, we relate E_{iso} to the expected number of neutrino events, μ , observed at IceCube. To do this, we need to take into account IceCube's effective area, $A_{\text{eff}}(E, \delta)$, which is strongly dependent on decl., and we also marginalize over the 3D

position of the source,

$$\begin{aligned} \mu &= \int A_{\text{eff}}(E, \delta) \Phi(E) P(\Omega, r) \Delta t dE dV \\ &= \sum_{i=0}^N p(\Omega_i) \int A_{\text{eff}}(E, \delta_i) \frac{E_{\text{iso}} E^{-2}}{4\pi \ln \left(\frac{E_2}{E_1} \right)} \\ &\quad dE \int_0^\infty \frac{1}{r^2} p(r|\Omega_i) dr, \end{aligned} \quad (4)$$

where the summation is over the pixels in the skymap of the GW event, $P(\Omega, r)$ is the 3D location PDF of the GW source, and $p(\Omega_i)$ is the probability per pixel. Since $p(\Omega_i)$ is a discrete quantity, we transform the integral into a sum over the pixels in the sky. The quantity $p(r|\Omega_i)$ is the per-pixel luminosity distance distribution of the form

$$p(r|\Omega_i) = \frac{r^2 d_{\text{norm},i}}{\sqrt{2\pi} d_{\sigma,i}^2} \exp \left[-\frac{(r - d_{\mu,i})^2}{2d_{\sigma,i}^2} \right], \quad (5)$$

where $d_{\text{norm},i}$, $d_{\mu,i}$, and $d_{\sigma,i}$ are parameters fitted in the i th pixel to create a per-pixel distance distribution. For details on the LIGO-Virgo skymaps and localizations, see Singer et al. (2016).

Using these distributions, we can numerically solve for the expected number of neutrino events at IceCube after marginalizing the localization uncertainty. We then perform trials with additional signal injection to compute a 90% UL on E_{iso} . The results for this calculation are shown in Table 1. This E_{iso} limit was only computed with the maximum-likelihood analysis described in Section 2.1. See Veske et al. (2020) for the LLAMA search's E_{iso} limits for the first three GW events with a different statistical treatment.

Figure 3 shows the ULs on E_{iso} as a function of the median distance to the source marginalized over the sky. The gray band in the figure represents the range of median ULs IceCube can set based on the best and worst point-source sensitivities shown in Figure 1. These ULs are computed using Equation (3), where $\Phi_0 \Delta t E_0^2$ is taken to be the minimum and maximum point-source sensitivities, respectively. We assume the point source has a precise distance measure, r , and a precise location on the sky.

We see that the ULs for all 11 GW events fall within this band and scale roughly with r^2 , as expected from geometric arguments. The scatter among the ULs is explained by IceCube's significant decl. dependence and the uncertainties in the distance measurements of the GW sources. Note that the ULs need not lie in this band in all cases. This band is representative of point sources with no 3D localization uncertainty. Nevertheless, the ULs should lie around the band, as our analyses rely strongly on IceCube's capability to detect high-energy neutrinos. Also shown in Figure 3 is the total radiated energy for each GW, which is calculated by taking the difference of the total rest mass of the progenitors and the final rest mass of the remnant object. We also plot the total rest mass energy of the initial binary system for reference. Our E_{iso} ULs show that the UL on the total energy radiated in high-energy neutrinos within the 1000 s time window is up to 2 orders of magnitude smaller than the total radiated energy of the binary system, while for some events, it is about the same order of magnitude.

4. Conclusion

Advances in detector technologies used in GW, electromagnetic, and neutrino astronomy have led to a scientific

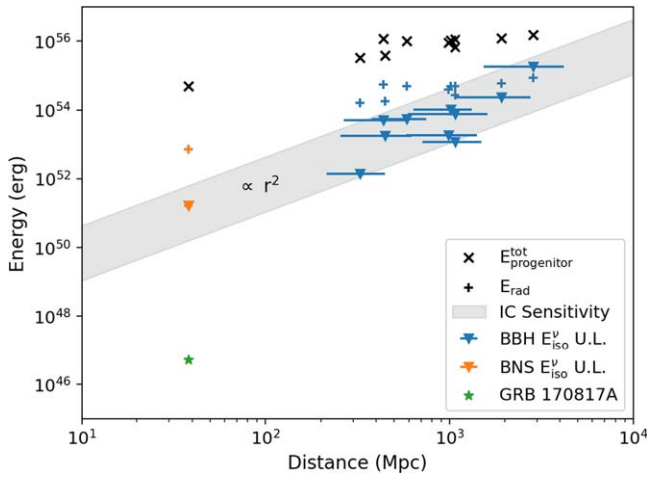


Figure 3. The 90% UL on the isotropic equivalent energy emitted in high-energy neutrinos during a 1000 s time window (blue and orange triangles). Here $E_{\text{progenitor}}^{\text{tot}}$ (black cross) is the total rest mass energy of the progenitors and E_{rad} (orange/blue plus signs) is the total radiated energy of the binary system. While not all of the progenitor energy is available for acceleration processes, we show it here as a relevant energy scale in the binary system. The median distances and 90% credible intervals are taken from the first GW catalog (Abbott et al. 2019). The distance errors for GW170817 are much smaller than the BBHs because of the precise measurements of the host galaxy (Cantiello et al. 2018). Note that the distance error bars also apply to the E_{rad} and $E_{\text{progenitor}}^{\text{tot}}$ measurements but are not shown here for clarity. Shown in green is the measured E_{iso} for GRB 170817A by the Fermi GBM taken from Abbott et al. (2017b). The gray band represents the range of 90% E_{iso} ULs that IceCube can set based on the range of point-source sensitivities shown in Figure 1.

revolution, rapidly expanding the fields’ cosmic and scientific horizons. Finding evidence of a joint GW–neutrino source would further expand our understanding of the sources of high-energy neutrinos and the energetic outflows driven by the interaction of compact objects.

We performed two different searches for neutrino emission from the 11 compact binary mergers in the first GW transients catalog, GWTC-1, from LIGO-Virgo. We found no significant neutrino emission from any of the 11 GW events and therefore placed ULs on the energy-scaled time-integrated neutrino flux (see Table 1). In addition to ULs on neutrino flux, we placed ULs on the isotropic equivalent energy emitted in neutrinos, E_{iso} , during the 1000 s time window (see Table 1). These limits show that BBH mergers emit up to 2 orders of magnitude less energy in high-energy neutrinos than they do in GWs. For the one BNS merger, GW170817, the UL on the energy emitted in neutrinos is about 2 orders of magnitude lower than the energy radiated in GWs. We also compared to measurements of the energy emitted in gamma-rays of the associated short gamma-ray burst, GRB 170817A. The Fermi GBM reported a UL on E_{iso} that is over 6 orders of magnitude lower than the energy radiated in GWs and over 4 orders of magnitude lower than the UL on the energy emitted in neutrinos (Abbott et al. 2017b).

In addition to searching for neutrino emission from the 11 mergers in GWTC-1, there are two pipelines implementing the two methods described in Section 2 in low latency during the O3 observing run. These low-latency searches are particularly useful in informing electromagnetic observatories where to point to search for optical counterparts. These analyses are described in detail in Hussain et al. (2019) and Countryman et al. (2019) and will be the subject of a future publication.

Searches for neutrino emission from longer time windows are also ongoing. These searches target neutrino emission from BNSs or neutron star–black hole mergers on a 2 week timescale. Neutrinos from kilonovae or ejected material from mergers involving neutron stars are potential sources of high-energy neutrinos for weeks after the initial merger (Kimura et al. 2018; Fang & Metzger 2017). Our sample of potential joint GW and neutrino sources continues to grow as more compact binary mergers are detected. With the 5–6 \times higher statistics expected in O3 (Abbott et al. 2018), we can search for a possible underlying population of joint sources.

The IceCube collaboration acknowledges the significant contributions to this manuscript from Raamis Hussain and Doğa Veske. The authors gratefully acknowledge the support of the following agencies and institutions: USA—U.S. National Science Foundation Office of Polar Programs, U.S. National Science Foundation Physics Division, Wisconsin Alumni Research Foundation, Center for High Throughput Computing (CHTC) at the University of Wisconsin–Madison, Open Science Grid (OSG), Extreme Science and Engineering Discovery Environment (XSEDE), U.S. Department of Energy National Energy Research Scientific Computing Center, Particle Astrophysics Research Computing Center at the University of Maryland, Institute for Cyber-Enabled Research at Michigan State University, and Astroparticle Physics Computational Facility at Marquette University; Belgium—Funds for Scientific Research (FRS-FNRS and FWO), FWO Odysseus and Big Science programmes, and Belgian Federal Science Policy Office (Belspo); Germany—Bundesministerium für Bildung und Forschung (BMBF), Deutsche Forschungsgemeinschaft (DFG), Helmholtz Alliance for Astroparticle Physics (HAP), Initiative and Networking Fund of the Helmholtz Association, Deutsches Elektronen Synchrotron (DESY), and High Performance Computing Cluster of the RWTH Aachen; Sweden—Swedish Research Council, Swedish Polar Research Secretariat, Swedish National Infrastructure for Computing (SNIC), and Knut and Alice Wallenberg Foundation; Australia—Australian Research Council; Canada—Natural Sciences and Engineering Research Council of Canada, Calcul Québec, Compute Ontario, Canada Foundation for Innovation, WestGrid, and Compute Canada; Denmark—Villum Fonden, Danish National Research Foundation (DNRF), Carlsberg Foundation; New Zealand—Marsden Fund; Japan—Japan Society for Promotion of Science (JSPS) and Institute for Global Prominent Research (IGPR) of Chiba University; Korea—National Research Foundation of Korea (NRF); Switzerland—Swiss National Science Foundation (SNSF); United Kingdom—Department of Physics, University of Oxford.

The authors are grateful for the LIGO Scientific Collaboration review of this Letter, and this Letter is assigned a LIGO DCC number (P2000092). The Columbia Experimental Gravity group is grateful for the generous support of Columbia University, in the City of New York, for National Science Foundation grant PHY-1708028, and for computational resources provided by the LIGO Laboratory (supported by NSF grants PHY-0757058 and PHY-0823459). D.V. is grateful to the PhD grant of the Fulbright foreign student program. I.B. is grateful for the generous support of the National Science Foundation under grant PHY-1911796, the Alfred P. Sloan Foundation, and the University of Florida.

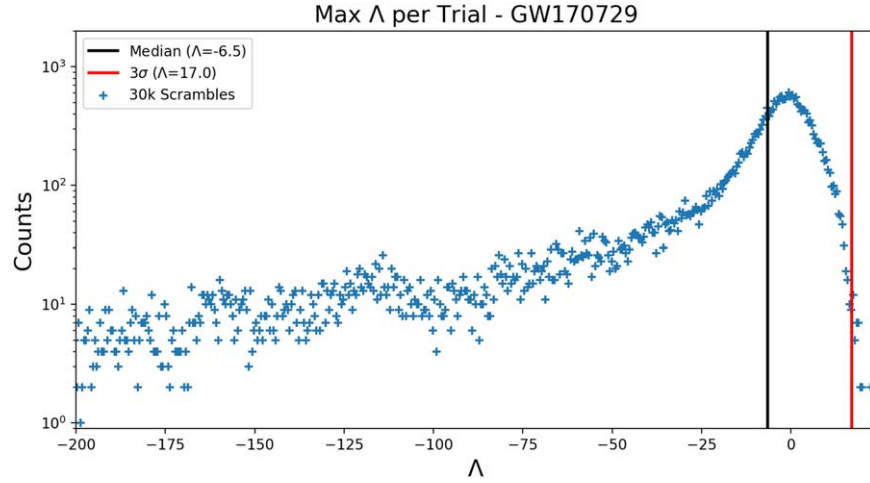


Figure A1. Background TS distribution for GW170729. We see a large fraction of Λ values that are negative due to most neutrino events on the sky being heavily down-weighted by the spatial weight.

Appendix

A.1. Maximum-likelihood Analysis

Figure A1 shows the background distribution for the unbinned maximum-likelihood analysis. Here 30,000 trials are performed for GW170729. Neutrino arrival times are randomly assigned, which has the effect of assigning a random R.A. value to each neutrino while preserving the decl. and temporal distribution of our data. Since IceCube’s sensitivity does not depend on R.A., we can randomize neutrinos in R.A. to produce different realizations on the sky.

For each trial and random realization of the sky, the likelihood is maximized in each pixel on the sky, and the maximum resulting TS on the sky is taken as the TS for that trial. Shown in Figure A1 are the maximum TS values on the sky for 30,000 unique trials.

Figure A2 shows the method used to compute sensitivity and ULs in the unbinned maximum-likelihood analysis. We perform signal injection trials with neutrinos from Monte Carlo. For each trial, we choose a random location on the sky weighted by the GW localization and inject signal. We compute a passing fraction that refers to how many trials yielded a TS larger than the background median for a given injected flux. We increase the injected flux and perform trials again. We repeat this procedure for multiple injected flux values and fit a χ^2 cumulative distribution function (CDF) to the passing fraction versus injected flux, as shown in Figure A2. In the case of computing ULs, the passing fraction refers to how many trials yielded a TS larger than the observed TS for the GW. We fix the lower bound of the UL to the sensitivity to be conservative.

A.2. LLAMA

The fluence ULs of the LLAMA search in Table 1 are calculated as follows. Three sets of neutrino lists are prepared for each GW event. In the first set, the lists consist of only background neutrinos whose count is drawn from a Poisson distribution with the mean background neutrino count in 1000 s. The neutrinos are chosen from the archival GFU data set. Neutrinos’ R.A.s and detection times are randomized and other properties are kept the same. The detection times of these

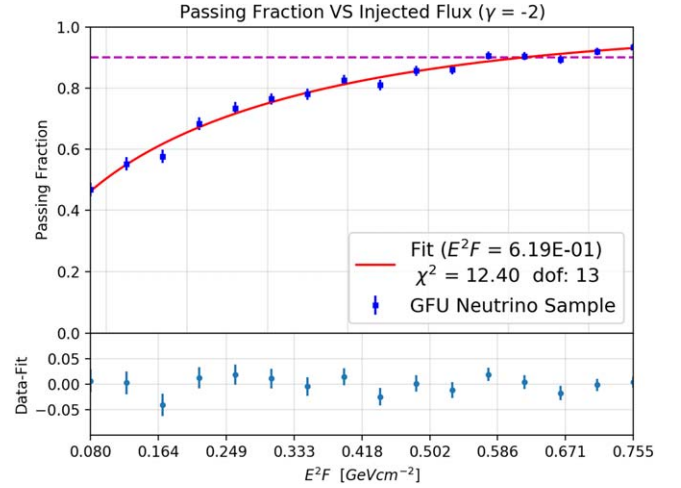


Figure A2. The 90% sensitivity flux for GW170729, computed by injecting an increasing neutrino flux according to an E^{-2} power-law spectrum and calculating the fraction of trials that return an observed Λ greater than the median of the background distribution shown in Figure A1. We use a χ^2 CDF to fit the data and compute the time-integrated flux, which gives a 90% passing fraction. This is defined as the sensitivity for the particular GW event.

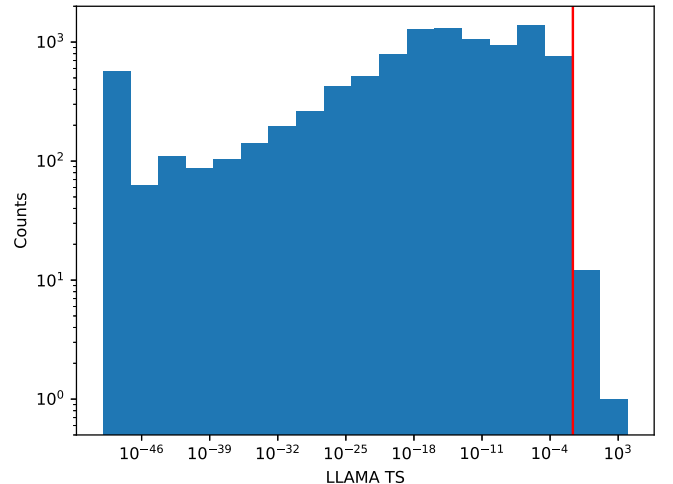


Figure A3. Background TS distribution of the LLAMA search for BBH mergers detected with the two aLIGO and the AdVirgo detectors at O2 sensitivity. Here TSs $< 10^{-50}$ are collected in the 10^{-50} bin. The red line shows the one-sided 3σ threshold.

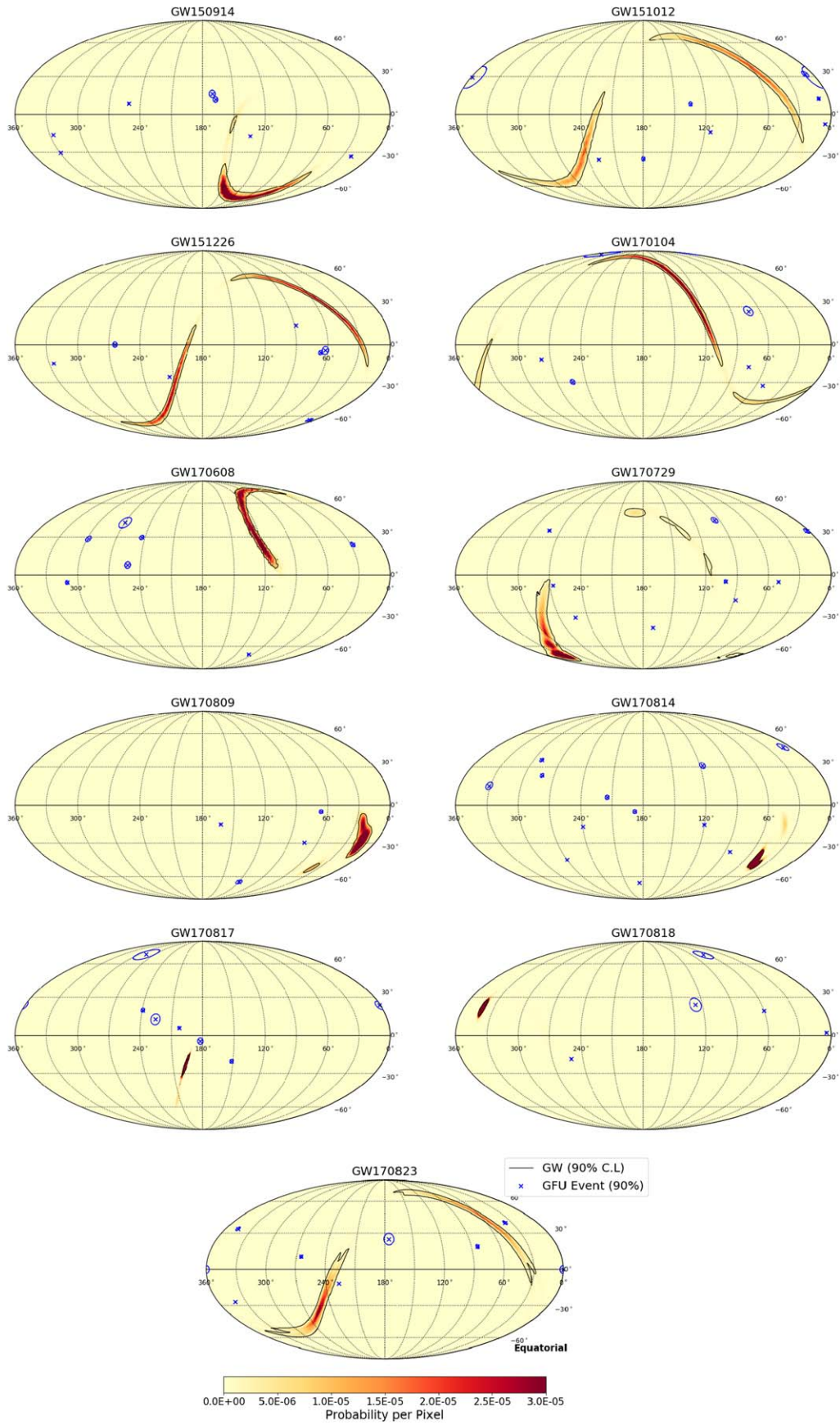






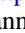
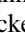




Figure A4. Skymaps for the 11 detected GW events overlaid with neutrinos within 1000 s of the GW trigger time.

neutrinos are uniformly chosen around the ± 500 s of the GW event time. The R.A.s are uniformly randomized between $[0, 2\pi]$. The second set of lists has one signal neutrino in addition to the first set of lists. The emission locations of the signal neutrinos are randomized according to the GW sky localization. The detection times of the neutrinos are chosen from a symmetric triangular distribution whose mode is the GW event time and extent is ± 500 s around the GW event time. The neutrinos are chosen from a Monte Carlo signal simulation list with an E^{-2} energy spectrum. The Monte Carlo list consists of neutrinos detected all over the sky. For choosing neutrinos from this list, only the neutrinos in the $\pm 1^\circ$ decl. band around the emission location are considered. The Monte Carlo list has an actual injection location, simulated detection location and simulated detection error on the localization for each simulated signal neutrino. Maintaining the difference between the actual injection and simulated detection location, chosen neutrinos' actual injection locations are shifted to emission points that have been chosen on the sky according to the GW's sky localization distribution. The third set of lists is similar to the second set of lists except for having two signal neutrinos emitted from the same point in each list. Then the analysis is run on these sets of lists. Finally, we find the fluence value for which 90% of the detected lists of neutrinos will have a higher TS than the TS of the actual detection. The fluence affects the expected number of signal neutrinos. The expected number of signal neutrinos for a fluence is found by using the effective area of the detector and assuming an E^{-2} spectrum. By using the TS values from the three sets of lists, we can calculate the fraction of events that would have a higher TS than the actual detection's TS for a fluence value. When doing this, we assume that the events that have three or more signal neutrinos will always have a higher TS than the actual detection's TS, since such a detection would be extremely significant. Moreover, we put a lower bound to the actual detection's TS that is equal to the median of the TS distribution of only background neutrinos (sensitivity). See Veske et al. (2020) for the limits obtained based on maximum-likelihood estimators without the sensitivity lower bound for the first three GW events.

Figure A3 shows the background TS distribution of the LLAMA search used for the analysis of joint GW high-energy neutrino events that have GWs detected by the three-detector network of two aLIGO detectors and the AdVirgo detector. In order to create background pairs of GWs and high-energy neutrino events, GWs were first injected and detected at O1/O2 sensitivity with the three GW detectors. The injections were made uniform in comoving volume. The injection volume is as large as the detectors' maximum reach. Then each detected GW injection was paired with a set of neutrinos whose count was drawn from a Poisson distribution whose mean was the mean count of the neutrino detections from the GFU stream in 1000 s. According to the Poisson draws, that many neutrinos were chosen from the archival GFU data set. Before the selection, the R.A. coordinates of the neutrinos in the data set were scrambled. Finally, those neutrinos were distributed uniformly in the ± 500 s window around the GW injections, which created the background joint GW high-energy neutrino event. The search was run on a set of $\sim 10^4$ such events.

ORCID iDs

I. Bartos  <https://orcid.org/0000-0001-5607-3637>
 J. J. DeLaunay  <https://orcid.org/0000-0001-5229-1995>
 R. Hussain  <https://orcid.org/0000-0002-3919-4426>
 U. Katz  <https://orcid.org/0000-0002-7063-4418>
 Z. Marka  <https://orcid.org/0000-0003-1306-5260>
 H. Pandya  <https://orcid.org/0000-0002-6138-4808>
 N. L. Strotjohann  <https://orcid.org/0000-0002-4667-6730>
 J. Vandenbroucke  <https://orcid.org/0000-0002-9867-6548>
 D. Veske  <https://orcid.org/0000-0003-4225-0895>
 T. Yuan  <https://orcid.org/0000-0001-5710-508X>

References

- Aartsen, M. G., Ackermann, M., Adams, J., et al. 2014, *PhRvD*, **90**, 102002
 Aartsen, M. G., Ackermann, M., Adams, J., et al. 2017a, *JInst*, **12**, P03012
 Aartsen, M. G., Ackermann, M., Adams, J., et al. 2017b, *Aph*, **92**, 30
 Aartsen, M. G., Ackermann, M., Adams, J., et al. 2018, *Sci*, **361**, 147
 Aartsen, M. G., Ackermann, M., Adams, J., et al. 2020, *PhRvL*, **124**, 051103
 Aasi, J., Abbott, B. P., Abbott, R., et al. 2015, *CQGrA*, **32**, 074001
 Abbott, B., Abbott, R., Abbott, T., et al. 2019, *PhRvX*, **9**, 031040
 Abbott, B. P., Abbott, R., Abbott, T. D., et al. 2016, *PhRvL*, **116**, 061102
 Abbott, B. P., Abbott, R., Abbott, T. D., et al. 2017a, *ApJ*, **848**, L12
 Abbott, B. P., Abbott, R., Abbott, T. D., et al. 2017b, *ApJ*, **848**, L13
 Abbott, B. P., Abbott, R., Abbott, T. D., et al. 2018, *LRR*, **21**, 3
 Abbott, B. P., Abbott, R., Abbott, T. D., et al. 2019, *ApJ*, **875**, 161
 Abe, K., Bronner, C., Hayato, Y., et al. 2018, *ApJL*, **857**, L4
 Adrián-Martínez, S., Albert, A., André, M., et al. 2016, *PhRvD*, **93**, 122010
 Adrián-Martínez, S., Samarai, I. A., Albert, A., et al. 2013, *JCAP*, **6**, 008
 Albert, A., André, M., Anghinolfi, M., et al. 2017a, *ApJL*, **850**, L35
 Albert, A., André, M., Anghinolfi, M., et al. 2017b, *PhRvD*, **96**, 022005
 Albert, A., André, M., Anghinolfi, M., et al. 2019, *ApJ*, **870**, 134
 Alexandreas, D., Berley, D., Biller, S., et al. 1993, *NIMPA*, **328**, 570
 AMON 2019, AMON IceCube Gold/Bronze, https://gcn.gsfc.nasa.gov/amon_icecube_gold_bronze_events.html
 Ando, S., Baret, B., Bartos, I., et al. 2013, *RvMP*, **85**, 1401
 Aso, Y., Márka, Z., Finley, C., et al. 2008, *CQGrA*, **25**, 114039
 Avrorin, A. D., Avrorin, A. V., Aynutdinov, V. M., et al. 2018, *JETPL*, **108**, 787
 Baret, B., Bartos, I., Bouhou, B., et al. 2011, *Aph*, **35**, 1
 Baret, B., Bartos, I., Bouhou, B., et al. 2012, *PhRvD*, **85**, 103004
 Bartos, I., Brady, P., & Márka, S. 2013, *CQGrA*, **30**, 123001
 Bartos, I., Dasgupta, B., & Márka, S. 2012, *PhRvD*, **86**, 083007
 Bartos, I., Finley, C., Corsi, A., & Márka, S. 2011, *PhRvL*, **107**, 251101
 Bartos, I., Veske, D., Keivani, A., et al. 2019, *PhRvD*, **100**, 083017
 Cantello, M., Jensen, J. B., Blakeslee, J. P., et al. 2018, *ApJ*, **854**, L31
 Cassidy, G., Cooper, R., Dawson, B. R., et al. 1989, *PhRvL*, **62**, 383
 Countryman, S., Keivani, A., Bartos, I., et al. 2019, arXiv:1901.05486
 Fang, K., & Metzger, B. D. 2017, *ApJ*, **849**, 153
 Formaggio, J. A., & Zeller, G. P. 2012, *RvMP*, **84**, 1307
 Górski, K. M., Hivon, E., Banday, A. J., et al. 2005, *ApJ*, **622**, 759
 GraceDB 2019, GraceDB Latest, <https://gracedb.ligo.org/latest/>
 Hussain, R., Vandenbroucke, J., & Wood, J. 2019, Proc. ICRC (Madison, WI), **36**, 918
 Keivani, A., Veske, D., Countryman, S., et al. 2019, Proc. ICRC (Madison, WI), **36**, 930
 Kimura, S. S., Murase, K., Bartos, I., et al. 2018, *PhRv*, **D98**, 043020
 Kintscher, T. 2016, *J. Phys. Conf. Ser.*, **718**, 062029
 LIGO Collaboration Virgo Collaboration 2008, *CQGrA*, **25**, 114051
 Petkov, V. B., Novoseltseva, R. V., Boliev, M. M., et al. 2018, *JETPL*, **107**, 398
 Razzaque, S., Mészáros, P., & Waxman, E. 2003, *PhRvD*, **68**, 083001
 Schumacher, L. 2019, *EPJWC*, **207**, 02010
 Singer, L. P., Chen, H.-Y., Holz, D. E., et al. 2016, *ApJS*, **226**, 10
 Singer, L. P., & Price, L. R. 2016, *PhRvD*, **93**, 024013
 van Elewyck, V., Ando, S., Aso, Y., et al. 2009, *IJMPD*, **18**, 1655
 Veitch, J., Raymond, V., Farr, B., et al. 2015, *PhRvD*, **91**, 042003
 Veske, D., Márka, Z., Bartos, I., & Márka, S. 2020, *JCAP*, **2020**, 016
 Virgo Collaboration 2015, *CQGrA*, **32**, 024001